Evaporation-Controlled Self-Assembly of Silica Surfactant Mesophases

A. Gibaud,*,† D. Grosso,‡ B. Smarsly,§ A. Baptiste,† J. F. Bardeau,† F. Babonneau,‡ D. A. Doshi,§,⊥ Z. Chen,§ C. Jeffrey Brinker,§,|| and C. Sanchez‡

Laboratoire de Physique de l'Etat Condensé, Université du Maine, UMR 6087 CNRS, 72085 Le Mans Cedex 09 France, Laboratoire Chimie de la Matière Condensée, Université Pierre et Marie Curie, 4 place Jussieu, 75 252, Paris Cedex 05, France, Department of Chemical and Nuclear Engineering and Center for Micro-Engineered Materials, Advanced Materials Laboratory, University of New Mexico, 1001 University Boulevard SE, Albuquerque, New Mexico 87106, and Sandia National Laboratories, Albuquerque, New Mexico 87185

Received: December 4, 2002

Surfactant templated silica mesophases belong to the class of self-assembled materials that exhibit long range ordered two-dimensional (2D) hexagonal, three-dimensional (3D) hexagonal, or 3D cubic mesostructures when the composition of the initial deposited solution and its aging time have been optimized. Thin films of such mesophases with a thickness typically less than 300 nm are now routinely obtained by dip coating. In this study a reference solution was used with a chemical composition leading to the formation of thin films with a 3D hexagonal ($P6_3/mmc$) mesostructure by dip coating. Thick films (about 10 μm thick) were alternatively prepared by a evaporation-controlled self-assembly (ECSA) process and studied with grazing incidence small-angle X-ray scattering (GISAXS). In the ECSA process, the mesostructure was developed under slower evaporation conditions than for dip-coated films by finely tuning the ethanol/H_2O evaporation rate of the reference solution horizontally deposited on a silicon wafer. It is shown that the evaporation rate of the solvent is one of the key parameters that control the final mesostructure and can, under certain conditions, promote the formation of the cubic mesophase. The ability to precisely control such a structural arrangement on the mesoscale is of major interest for making sensor arrays, nanoreactors, photonic and fluidic devices, and low dielectric constant films.

Introduction

As a result of their large surface area, narrow pore size distribution and precisely tailored pore morphology, surfactant templated mesostructure silica thin films have received much attention because of their high potential applications as sensors, as optoelectronic devices, and in selective catalysis.[1−5] Such materials are prepared by combining sol gel chemistry with the texturation imposed by the surfactant physicochemistry in a procedure called EISA, "evaporation-induced self-assembly".[6] Silica thin films (50−500 nm thick) prepared from TEOS (tetraethyl orthosilicate) as the inorganic precursor in acidic media and CTAB (cetyltrimethylammonium bromide) as structure-directing agent exhibit lamellar, two-dimensional (2D) hexagonal ($p6m$), three-dimensional (3D) hexagonal ($P6_3/mmc$), or cubic ($Pm3n$) mesostructures.[3,7−9] The dynamic process that occurs during the film deposition/evaporation has been followed in situ by simultaneous grazing incidence small-angle X-ray scattering (GISAXS) and interferometry measurements.[7,8]

Recently, it has been reported that for dip-coated thin films the mesostructures are formed through a disorder−order transition. This transition may involve within the film intermediate hybrid mesophases that are related to a concentration gradient (CG).[8,10,11] In thin films, the initial CTAB/TEOS ratio, the extent of inorganic condensation before deposition, and the environmental relative humidity were found to be crucial parameters for tailoring the final mesostructure.[12] The influence of the evaporation rate of volatile entities, which has not yet been studied in detail, is obviously an additional key parameter that might determine the final mesostructure. Indeed, in the EISA method the evaporation of the solvent (i.e., ethanol) promotes progressive increase in the concentration of nonvolatile species, surfactant micelle formation, and their self-assembly with inorganic moieties (silica oligomers) present in the initial solution. For a given sol, the evaporation rate of ethanol and water depends on film thickness, external relative humidity (RH), partial vapor pressure of ethanol, temperature, and diffusivity of the volatile species (i.e., viscosity). Evaporation at the film/air interface results in a CG through the film. Due to the CG, the transformation of the surfactant−inorganic supramolecular arrangement into micelles first appears at the more concentrated interface (film/air).[11,13,14] In addition, the relative composition in EtOH, water, surfactant, and silica intermediates together with the mobility of entities related to viscosity vary locally in the direction perpendicular to the film surface as a function of time (and thickness). Since with CTAB the existence of the 3D phases (such as the 3D hexagonal or cubic) is likely restricted to narrow regions of the phase diagram, small changes in such parameters may have tremendous effects on the occurrence of these phases. Many combined scenarios can be thus inferred, and different structures can form simultaneously and independently during evaporation depending on

* To whom correspondence should be addressed. E-mail: gibaud@univ-lemans.fr.
† Université du Maine.
‡ Université Pierre et Marie Curie.
§ University of New Mexico.
|| Sandia National Laboratories.
⊥ Current address: Los Alamos National Laboratory, LANSCE 12, NM 87545.

10.1021/jp027612l CCC: $25.00
Published on Web 05/30/2003

the CG. For instance, phase transitions can be hindered due to too high a local viscosity.[13]

Despite the complexity of this process, we present a first insight of the role of the evaporation rate in the mesostructuralization process. This is made possible by studying the dynamics of organization using in situ time-resolved GISAXS experiments performed during thin and thick film processing from strictly identical initial sols and environment conditions, but in various evaporation rates that were imposed by an artificial vacuum-induced air convection.[13,14] Starting from a selected reference solution, we will see that one can obtain either the 2D hexagonal (*p*6*m*), the 3D hexagonal ($P6_3/mmc$), the cubic (*Pm*3*n*), or mixed structures depending on the evaporation conditions. This suggests that one fixed sol composition (same aging time) is wedded not to a single final hybrid mesophase but more to the pathway taken during the ECSA that is directly related to the competition between kinetics of condensation and of self-assembly.

Materials and Methods

A prehydrolyzed solution was prepared by refluxing for 1 h at 80 °C an ethanolic solution containing TEOS, deionized (DI) water, and hydrochloric acid in the following molar ratios 1 TEOS:3 EtOH:5 $\times$ 10^{-5} HCl:1 H_2O. CTAB dissolved in ethanol and an additional amount of acidic DI water was then added to this solution. The final molar ratio was 1 TEOS:20 EtOH:0.004 HCl:5 H_2O:0.1 CTAB.[7] This solution was then continuously stirred at 200 rpm and aged for 4 days at room temperature before starting the in and ex situ scattering experiments. Scattering experiments were performed at the 22B beam line (NSLS, Brookhaven National Laboratory). A monochromatic beam was deflected by a Ge(111) single crystal to impinge on the sample surface at an incidence close to 0.35°. By finely tuning the incident angle, it was possible to adjust the penetration depth in the sample. For in situ experiments the reference sol was poured on the surface of a 2 cm^2 silicon wafer to cover its surface.

In the following the films prepared by dropping the liquid onto the wafer are denoted as "thick" films since the initial and final film thickness were about 100 and 10 μm. The diffraction patterns were recorded on a MAR CCD 2D detector located 62 cm behind the sample. The evolution of the film structure was recorded every 15 s during the evaporation. Ex situ experiments were also carried out under controlled conditions of evaporation. To assist the EISA, a vacuum pump was connected to a cylindrical pipe (6 cm in diameter) sitting at given distances from a wafer covered with the desired solution. By varying the distance from the pipe to the sample, it was possible to adjust the rate of evaporation of the liquid film. The aperture of the vacuum pipe (8 cm diameter) was much larger than the sample surface, so the evaporation flow could be assumed to be laminar. The dried films obtained by this technique were then mounted on the sample stage of the diffractometer, and diffraction patterns were subsequently recorded. Thin films were prepared by dip coating silicon wafers in the same reference solution at a constant withdrawal speed of 14 cm/min. For all films, the relative humidity was maintained at 37% and temperature was 25 °C.

Results

Figure 1 shows a typical GISAXS pattern of a thin film about 300 nm thick (evaluated by ellipsometry) prepared by dip coating a silicon substrate in the initial sol. For such a thin film, the evaporation is extremely fast as the whole drying process takes place in less than 20 s. The dried film exhibits the typical pattern of the $P6_3/mmc$ (3D hex) structure. On the contrary, a

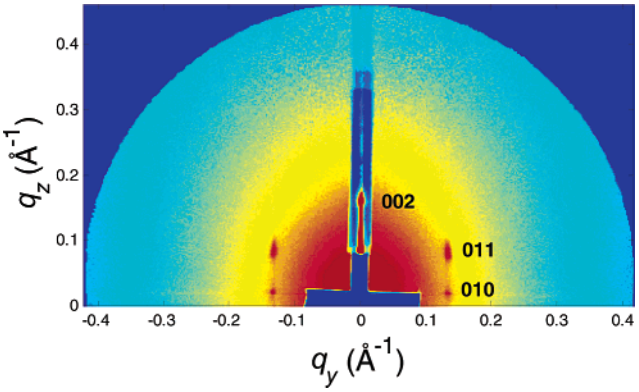

Figure 1. The 3D hex pattern obtained by dip coating.

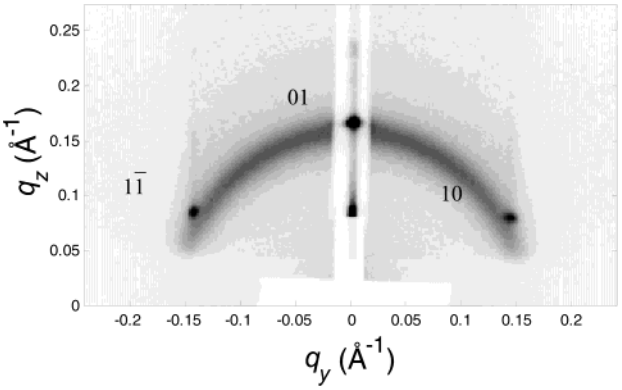

Figure 2. A 2D hex pattern superimposed on a wormlike structure obtained by slow evaporation.

film about 10 μm thick prepared by slow evaporation required a much longer drying time (of the order of 20 min). Its final mesostructure deduced from the GISAXS pattern shown in Figure 2 is typical of a *p*6*m* (2D hex) structure having part of the domains preferentially oriented with their tubular micelles aligned with the surface (diffraction peaks) and part randomly oriented (diffraction ring).[15] As previously reported, well-aligned domains are likely located at interfaces.[10] These results clearly show that the rate of ethanol evaporation is closely associated with the applied coating technique, to the initial quantity of sol, and to interface of exchange where the evaporation is carried out. This rate strongly influences the final structure.

With the aim to solely analyze the role of evaporation in a qualitative way, thick films were further prepared ex situ under the same initial conditions (same solution, quantity of matter, and RH) with a vacuum pump located at various distances from the film surface (2, 4, 6, and 8 cm). Under such conditions the evaporation rate and the related CG are accentuated by lowering the orifice of the vacuum pipe. As shown in Figure 3, GISAXS patterns obtained by such a vacuum assisted evaporation (VAE) technique depend on the distance *d* between the vacuum pipe orifice and the sample. 2D hexagonal patterns similar to the one shown in Figure 2 are observed at $d = 2$ and 4 cm (see Figure 3a,b). One can clearly see on these figures that the 2D hexagonal phase coexists with a wormlike structure that tends to vanish when *d* increases (decrease of the evaporation rate). Quantitative analysis of Figure 3a,b shows that the intensity ratio of the Bragg reflections (maximum peak intensity) to the ring increases roughly by a factor of 2 while the full width at half-maximum (fwhm) width of the Bragg reflections simultaneously decreases by 30%. This is a clear sign that in this range of distances the decrease of the evaporation rate favors a better organization since the wormlike structure disappears to the

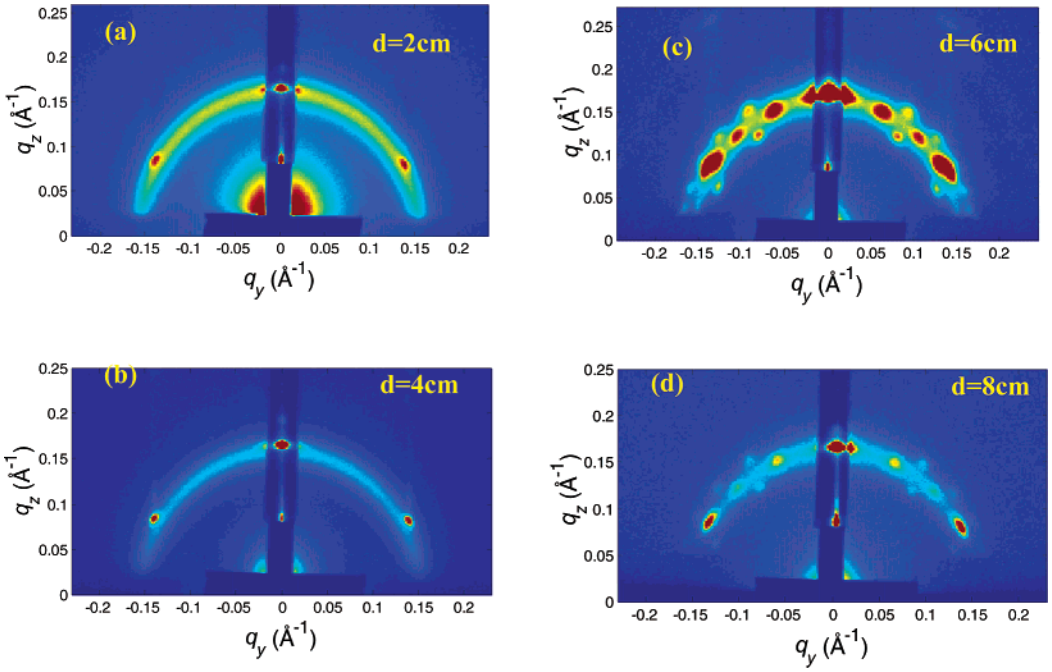

Figure 3. Ex situ GISAXS patterns obtained by VAE at different values of *d*. (a) $d = 2$ cm and (b) $d = 4$ cm, a wormlike structure superimposed on a 2D hex pattern; (c) $d = 6$ cm), a cubic structure; (d) $d = 8$ cm, a cubic structure.

TABLE 1: Different Structures Observed during the ECSA Process of the Same Solution When the Distance *d* Between the Film and the Vacuum Pump Is Varied

$d = 2$ cm	$p6m$, $a_{hex} = 44.2 \pm 1$ Å
$d = 4$ cm	$p6m$, $a_{hex} = 43.6 \pm 1$ Å
$d = 6$ cm	$Pm3n$, $a_{cub} = 93.6 \pm 2$ Å
$d = 8$ cm	$Pm3n + p6m$, $a_{cub} = 92.6 \pm 2$ Å
$d =$ Infinity	$p6m$, $a_{hex} = 41.2 \pm 1$ Å
dip coating	$P6_3/mmc$, $a_{hex} = 52.6 \pm 1$ Å, $c_{hex} = 76.8 \pm 2$ Å

benefit of the 2D hexagonal phase. This is further confirmed at $d = 6$ cm, where a cubic pattern corresponding to the *Pm*3*n* discontinuous cubic structure forms with domains preferentially oriented with their [121]* direction normal to the surface (see Figures 3c and 4). The cubic structure was reproducibly obtained as long as the distance from the sample to the vacuum pipe orifice was close to 6 cm. At $d = 8$ cm (Figure 3d), the cubic structure is still visible and probably coexists with the 2D hexagonal phase.

We can thus conclude from these observations summarized in Table 1 that VAE yields different mesophases and that the appearance of the cubic phase is associated with an optimal evaporation rate, standing within quite a narrow condition range. The orientation of the cubic phase with respect to the 2D hexagonal one can be understood if we consider that for symmetry reasons the (111) plane of the cubic phase should have the same orientation as the basal plane of the 2D hex phase. As shown in Figure 4 the (111) plane of the cubic phase can be oriented in the same way as the basal plane of the *p*6*m* structure by rotating the cubic phase clockwise by 45° about the [010]* direction and then rotating it clockwise by 35.7° about the [10$\bar{1}$]*. After these two rotations the (111) cubic plane will have the same orientation as the basal plane of the *p*6*m* 2D hex and one will find the [121]* direction along the normal to the surface of the film. Since in the *Pm*3*n* structure the reflections 121 and 120 are very intense, they dominate the scattering pattern. This is what is observed in Figure 4, where the 121 reflection is scattering in the specular Q_z direction normal to the surface of the film with a strong intensity (reduced by the presence of an absorber). Off-specular characteristic reflections of the cubic

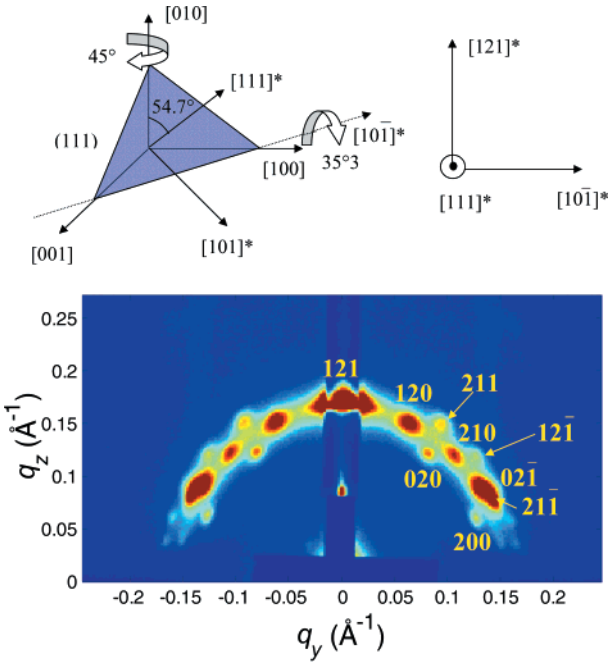

Figure 4. Explanation of the orientation of the cubic phase observed in the GISAXS pattern of Figure 3 together with the Miller indices of the Bragg reflections.

structure are also visible in the figure. The angular extension of the Bragg reflections definitely show that the cubic crystallites exhibit a large mosaic spread.

The characterization of the pathway through which the cubic final mesotructure was attained by in situ measurements. As shown in Figure 5, at $d = 6$ cm the cubic structure is formed from a micellar disordered phase ($t = 60$ s) which partially adopts the *p*6*m* structure at $t = 75$ s before transforming into the cubic *Pm*3*n* phase at $t = 750$ s via a common orientation of the basal plane of the *p*6*m* structure with the (111) plane of the cubic one.[16] A consequence of such a relation is that the two 10 and 01 Bragg reflections of the *p*6*m* pattern must be located at the same position as the 121 and the 21$\bar{1}$ of the *Pm*3*n*,

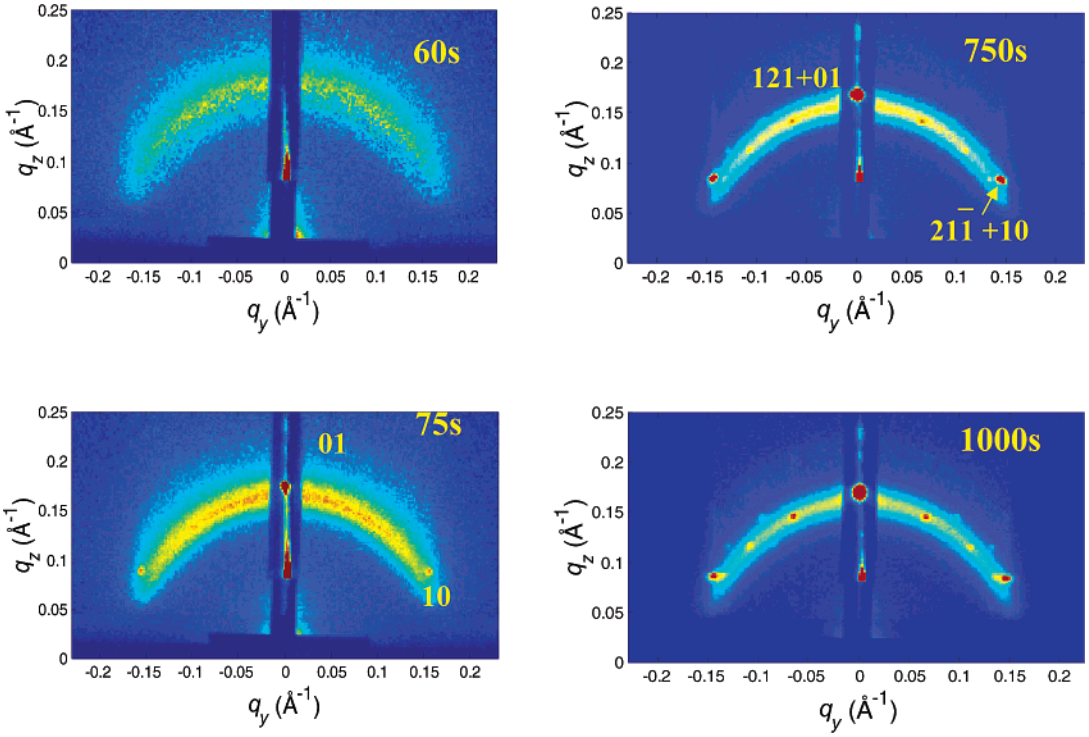

Figure 5. In situ GISAXS pattern obtained by VAE at $d = 6$ cm showing the pathway through which the final cubic structure is formed: at $t =$ 60 s, micellar phase (a, top left); at $t = 75$ s, observation of 2D hex pattern (b, bottom left); at $t = 750$ s (c, top right) and $t = 1000$ s (d, bottom right), cubic structure together with 2D hex structure. The places where the reflections of the cubic phase coexist with the one of the hexagonal phase are indicated in (c). All the images are recorded for an incident angle of 0.35°.

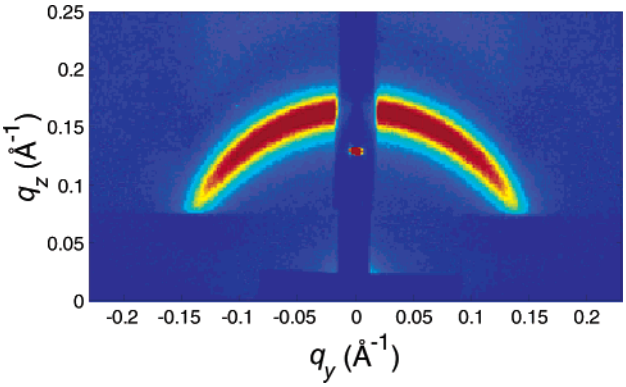

Figure 6. GISAXS pattern of the film corresponding to Figure 5d taken at an incidence of 0.9°. The penetration depth is much larger in this case, and the pattern mainly shows a wormlike structure.

respectively, overlapping each other. The observation of a ring superimposed on the characteristic reflections of the *p*6*m* and *Pm*3*n* ordered structures clearly shows that the film is not uniform in composition. By varying the incident angle, it was possible to show that the top part of the film was composed of the cubic structure (small angle of incidence) whereas the bottom part corresponded to the wormlike structure (large angle of incidence; see Figure 6). This is clear evidence that the structure at the two interfaces is not the same and that the 3D structure is favored at the solvent-poor top interface (fast evaporation). Other experiments performed on similar systems in which two phases coexist in the film (such as 2D hex + wormlike or 3D cubic + 2D hex) always show that the phase having the highest symmetry is at the top part of the film.

Discussion

Since the complete set of chemical parameters and the experimental procedure were kept identical except for the evaporation rate of the solvent, one can conclude in view of these results that the solvent evaporation rate plays a key role in the structuralization of the deposited films. While with CTAB it is relatively easy to obtain a 2D hex phase by the EISA method as long as the initial sol composition and its aging time are chosen appropriately, ending up with a 3D phase is far more difficult and the processing conditions must be carefully adjusted. When the rate of evaporation is controlled during the self-assembly process, the EISA method becomes the evaporation-controlled self-assembly (ECSA) process. This study clearly shows that different rates of evaporation yield final structures that are not necessarily single-phased but are composed of domains either with different degrees of orientation (typical for *p*6*m* structure) or with different structures (*Pm*3*n* often accompanied by *p*6*m* and wormlike).

Explaining these results is made possible by introducing the role of CG produced at different rates of evaporation. A fast evaporation induces a large CG, whereas a slow one will favor a more homogeneous solution. For large CG, multiphase systems are likely to be observed since the films do not have the same chemical composition at both interfaces. In particular, since ethanol evaporates faster at the air/film compared to ethanol within the film, the top part of the film is ethanol deficient. Therefore, an intermediate phase can be trapped at this interface as a result of too poor a mobility induced by the lack of solvent and by the condensation of the inorganic phase promoted by the connection of the inorganic species. For the *p*6*m* structure ($d = 2$ and 4 cm), the intensity of the Bragg peaks increases when the evaporation rate decreases while the ring intensity inversely decreases. This means that a higher degree of orientation is favored for lower rate of evaporation. This can be explained in terms of too high a local rigidity (higher rate of evaporation is associated with a greater concentration gradient and more rigid interface) and less time to permit the rearrangement for fast systems.

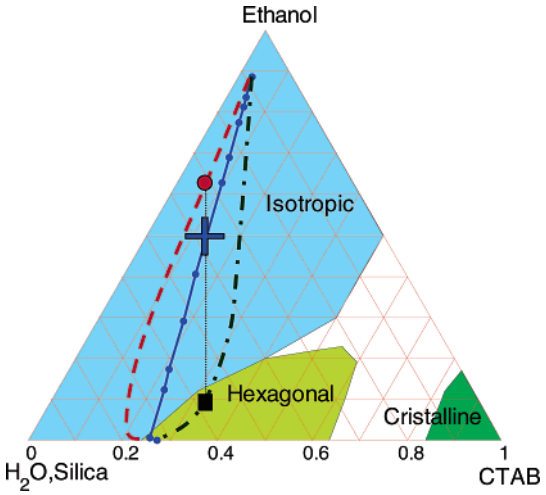

Figure 7. Representation of pathway taken during the slow evaporation of the solvent: average evolution of the film (full line), ethanol-rich bottom part of the film (dashed line), and ethanol-deficient top part of the film (dashed−dotted line). The cross gives the average composition of the film in the phase diagram while the square and the circle symbols indicate the composition of the top and bottom parts, respectively. Apart from the pathway taken by the average film,[13,14] the two other pathways drawn in this figure are just a guide to the eye to support the discussion presented in the text (they do not correspond to specific measurements).

According to Fontell et al.,[17] discrete micelles, composing the present cubic structure, are favored in ethanol-free media. However, water molecules located at the hydrophilic boundary of the micelles are necessary to increase the curvature of the micelles. As recently reported,[18] ethanol is first eliminated from the film and then water (depending on the relative humidity). The departure of water is then delayed, and if the film at the air interface is poor enough in ethanol and rich enough in water (reached by the medium evaporation rate process) at a specific time where the network is flexible enough and the surfactant composition is such that spherical micelles can be accommodated (cylinder-to-sphere transformation), the formation of the cubic phase takes place at this interface and may be retained for the rest of the drying by the constant evaporation regime controlled by the diffusion of ethanol molecules. Eventually, further evaporation promotes silica condensation which tends to freeze the structure. This explanation is in perfect agreement with the recent results obtained by Cagnol et al. on the role of humidity that promotes the appearance of the cubic phase.[12]

As shown in Figure 7, all the features observed in this study can be qualitatively understood if one considers that the CG promotes different pathways inside the film. Referring to the phase diagram presented by Fontell et al.,[17] the mean evolution of the film composition can be drawn from the evolution of the evaporated mass of solvent.[13,14] However, with respect to the average pathway the top part of the film being deficient in ethanol will take the lower pathway while the bottom part rich in ethanol will take the upper one. If the silica condensation is quick enough, different phases corresponding to the different pathways can be trapped inside the film. The quantitative understanding of this complex situation would necessitate the temporal and spatial composition of the film (water, ethanol, surfactant, silica) in the direction perpendicular to the substrate.

Conclusions

In this study, a reference solution aged for 5 days was used to dip coat thin films (of thickness $t < 300$ nm). With the specific composition of this reference solution, the dip-coated films exhibited 3D hexagonal structure with $P6_3/mmc$ symmetry. Thicker films (of thickness $t \sim 10$ μm) were alternatively produced under different evaporation conditions from the same reference solution. We have observed that the final structure of the film is strongly influenced by the rate of evaporation which itself governs the CG inside the film. All the common phases (wormlike, *p*6*m*, *Pm*3*n*) usually observed in surfactant templated silica thin films were obtained by ECSA. By varying the incident angle of the X-ray beam, we show that different phases may coexist inside the film with usually the highest symmetry phase located at the top part of the film. The observation of the cubic *Pm*3*n* structure was found to be subtly related to the delicate competition between the evaporation rate of the solvent, the water diffusion, and the silica condensation. Such drastic conditions were allowed by a careful tuning of the evaporation rate that is controlled here by the distance *d* from the vacuum pipe to the sample. The influence of the CG on the observation of different phases is inferred to be related to alternate pathways taken during the evaporation and is discussed in the framework of the phase diagram.

Acknowledgment. This work was supported by the French ACI "Nanostructure" under Project No. 03-01, the UNM/NSF Center for Micro-Engineered Materials, the AFOSR, the DOE Basic Energy Sciences Program, and SNL's Laboratory Directed R&D program. Research carried out in part at the National Synchrotron Light Source, Brookhaven National Laboratory, is supported by the U.S. Department of Energy, Division of Materials Sciences and Division of Chemical Sciences.

References and Notes

(1) Beck, J. S.; Vartuli, J. C.; Roth, W. J.; Leonovicz, M. E.; Kresge, C. T.; Shimtt, K. D.; Chu, C. T.-W.; Olson, D. H.; Sheppard, E. W.; McCullen, S. B.; Higgins, J. B.; Schlenker, J. L. *J. Am. Chem. Soc.* **1992**, *114*, 10834.

(2) Yang, H.; Coombs, N.; Sokolov, I.; Ozin, G. A. *Nature* **1996**, *381*, 549.

(3) Lu, Y.; Ganguli, R.; Drewien, C. A.; Anderson, M. T.; Brinker, C. J.; Gong, W.; Guo, Y.; Soyez, H.; Dunn, B.; Huang, M. H.; Zink, J. I. *Nature* **1997**, *389*, 364.

(4) Brinker, C. J. *Curr. Opin. Colloid Interface Sci.* **1998**, *3*, 166−173.

(5) Zhao, D.; Yang, P.; Melosh, N.; Feng, J.; Chmelka, B. F.; Stucky, G. D. *Adv. Mater.* **1998**, *10*, 1380.

(6) Brinker, C. J.; Lu, Y.; Sellinger, A.; Fan, H. *Adv. Mater.* **1999**, *11*, 579.

(7) Grosso, D.; Balkenende, A. R.; Albouy, P. A.; Lavergne, M.; Babonneau, F. *J. Mater. Chem.* **2000**, *10*, 2085.

(8) Grosso, D.; Babonneau, F.; Albouy, P. A.; Amenitsch, H.; Balkenende, A. R.; Brunet-Bruneau, A.; Rivory, J. *Chem. Mater.* **2002**, *2*, 931.

(9) Besson, S.; Gacoin, T.; Jacquiot, C.; Ricolleau, C.; Babonneau, D.; Boilot, J.-P. *J. Mater. Chem.* **2000**, *10*, 1331.

(10) Grosso, D.; Balkenende, A. R.; Albouy, P. A.; Ayral, A.; Amenitsh, H.; Babonneau, F. *Chem. Mater.* **2001**, *13*, 1848.

(11) Grosso, D.; Babonneau, F.; de A. A. Soler-Illia, G. J.; Albouy, P. A.; Amenitsch, H. *Chem. Commun.* **2002**, 748.

(12) Cagnol, F.; Grosso, D.; de A. A. Soler Illia, J. G.; Crepaldi, E. L.; Babonneau, F.; Albouy, P. A.; Amenitsch, H.; Sanchez, C. *J. Mater. Chem.*, in press.

(13) Gibaud, A.; Doshi, D.; Ocko, B.; Goletto, V.; Brinker, C. J. Presented at 3IMMS Korea 2002, in press.

(14) Doshi, D.; Gibaud, A.; Goletto, V.; Lu, M.; Gerung, H.; Hang, S.; Ocko, B.; Brinker, C. J. Submitted for publication in *Nat. Mater.*

(15) Klotz, M.; Albouy, P. A.; Ayral, A.; Ménager, C.; Grosso, D.; Van der Lee, A.; Cabuil, V.; Guizard, C. *Chem. Mater.* **2000**, *12*, 1721.

(16) Che, S.; Kamiya, S.; Terasaki, O.; Tatsumi, T. *J. Am. Chem. Soc.* **2001**, *123*, 12089.

(17) Fontell, K.; Khan, A.; Lindstrom, B.; Maciejweska, D.; Puang-Ngern, S. P. *Colloid Polym. Sci.* **1991**, *269*, 7.

(18) Huang, M. H.; Soyez, H. M.; Dunn, B. S.; Zink, J. I. *Chem. Mater.* **2000**, *12*, 231.